

# Synergizing Experimentation and Computation: Predicting Energetic Potential in New Cyclo-Peroxide Compounds

Mazal Rachamim, Amiram Goldblum, and Abraham J. Domb\*



Cite This: *ACS Omega* 2024, 9, 42746–42756



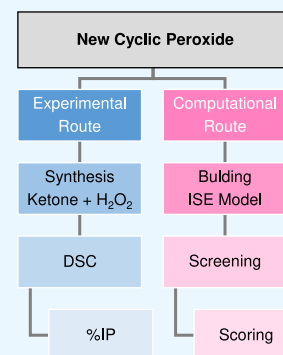
Read Online

ACCESS |

Metrics & More

Article Recommendations

**ABSTRACT:** This manuscript explores the synthesis of new cyclo-peroxide compounds (CPs) through a systematic approach involving 10 different ketones and two concentrations of H<sub>2</sub>O<sub>2</sub>. Following spectroscopic analysis and calorimetric tests on 10 selected compounds, the percentage of Power Index (%PI) was calculated. The study introduces a computational methodology based on the Iterative Stochastic Elimination (ISE) algorithm. The newly constructed ISE model, with demonstrated robust predictive capabilities indicated by its statistical parameters, was employed to screen and score the CPs, assessing their potential as energetic materials. Comparison between %PI obtained experimentally, and the ISE index derived computationally revealed consistent assessments of the new CPs' energetic potential. The research emphasizes that, particularly in the synthesis of cyclic peroxides, the ISE model is a preferable and efficient tool for predicting a compound's potential as an energetic substance. Utilizing the ISE model ensures faster, more cost-effective, and safer decision-making in experimental examinations, focusing attention only on compounds with the highest ISE scores. Furthermore, the manuscript suggests an intriguing avenue for future research by proposing the investigation of ester nitrates. The study advocates a comprehensive approach that combines experimental methods (synthesis, spectroscopy, and DSC) with computational evaluation using the ISE model to identify potential high-energy compounds. This integrated approach promises to enhance the efficiency and reliability of the energetic materials discovery process.



## 1. INTRODUCTION

High Energy Materials (HEMs) encompass chemical compounds or mixtures that rapidly decompose when triggered by external stimuli like heat, shock, friction, or ignition. This reaction results in a sudden release of substantial energy (an exothermic reaction) and the generation of expanding gas. The ensuing shock wave, intense heat, and the large volume of rapidly formed gases account for the destructive force of an explosion, often indicated by distinctive exothermic peaks in DSC thermograms. Examples of high-energy materials include explosives, fuels, and propellants.<sup>1–5</sup>

Explosives are classified diversely based on various criteria, as illustrated in Figure 1. They are broadly categorized into Primary and Secondary Explosives. Primary explosives, highly sensitive to shock, friction, and heat, detonate rapidly upon ignition. Secondary Explosives, less sensitive to these stimuli, ignite in small quantities but can also detonate. Secondary explosives, mostly composed of organic compounds, exhibit further classification based on functional groups.<sup>1,6,7</sup>

Improvised explosives, whether fertilizer-based (like ammonium nitrate) or peroxide-based (e.g., TATP, known as the 'mother of Satan'), are crafted outside of controlled environments. They've become pivotal resources for terrorists and criminals due to stringent regulations on conventional explosives and easy access to raw materials, necessitating heightened global security awareness.<sup>7–9</sup>

Peroxide-based explosives result from combining moderately concentrated hydrogen peroxide solutions with alkyl ketones, known as ketone precursors, in an acidic solution. This process initiates the production of cyclic peroxides with diverse substituents on carbon atoms.<sup>10</sup>

Organic cyclic structures are generally preferred over aliphatic ones from a thermodynamic standpoint. This preference emerges from the lower inherent potential energy in cyclic formations compared to their acyclic counterparts, making them more stable and, consequently, more thermodynamically favorable. However, within cyclic products, variations exist. For instance, under acid catalysis involving hydrogen peroxide and acetone, TATP (Triacetone triperoxide) emerges as the primary product. Changes in catalyst type, concentration, and reaction temperature show minimal impact on product composition, and DADP (Diacetone diperoxide) formation remains absent under these conditions. However, the transition from TATP to DADP arises in the presence of strong inorganic acids at elevated molar ratios

Received: April 16, 2024

Accepted: July 19, 2024

Published: October 11, 2024



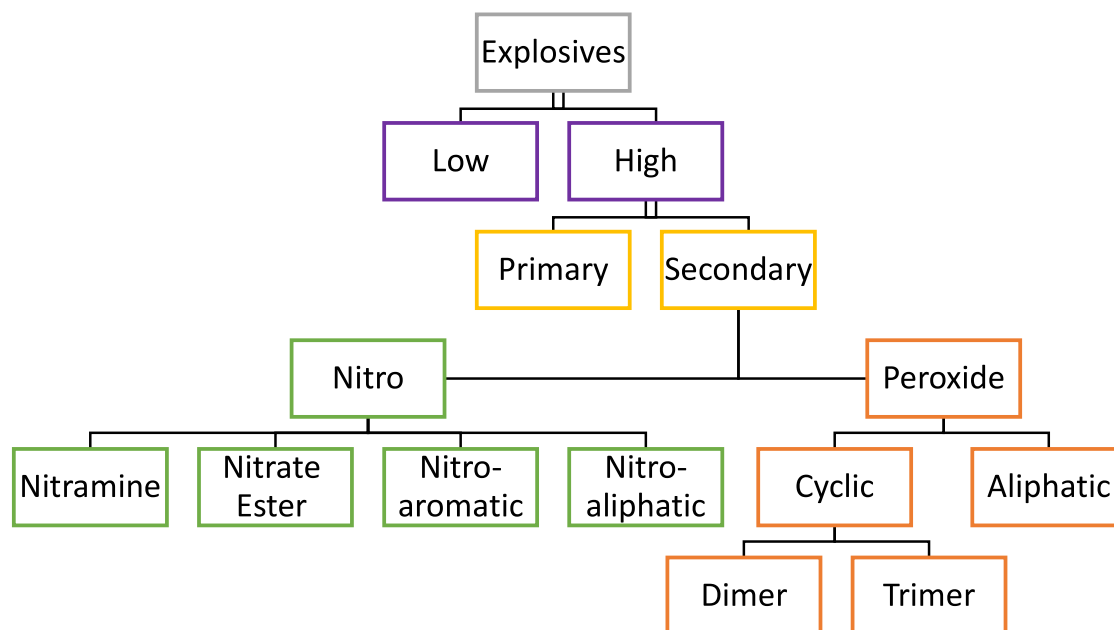


Figure 1. General classification of explosives.

( $n(\text{acid})/n(\text{acetone}) > 1$ ) when the mixture is allowed to stand in the acidic environment.<sup>11</sup> DADP is the thermodynamically favored product, while TATP is kinetically favored. Consequently, elevated reaction temperatures promote the production of DADP as the primary product over TATP.<sup>12</sup>

In our study, we pursued an exploration of novel organic peroxides through two distinct avenues: experimental and computational methodologies. Initially, peroxides were synthesized by combining hydrogen peroxide (in two different concentrations) with various ketones. Subsequent analyses, including Thin-Layer Chromatography (TLC) and spectroscopic techniques (FTIR, NMR, MS), were performed on the resulting compounds.

Utilizing Differential Scanning Calorimetry (DSC), we determined the detonation energy of these products, enabling the subsequent calculation of the Power Index (PI) for each case. The products were then ranked based on their relative explosive strengths, as derived from their PI values.

Concurrently, the Iterative Stochastic Elimination (ISE) algorithm was employed to screen these peroxides, assigning individual rankings. ISE is a generic algorithm designed to discover optimal solutions for highly complex combinatorial problems.<sup>13</sup> The primary candidates discovered by the ISE algorithm belong to the field of pharmaceuticals.<sup>14–19</sup> Over the past few years, our comprehensive study has explored the applicability of this algorithm in identifying potential candidates for new High Energetic Materials (HEMs). The received approval underscores its versatile capability in this regard.

## 2. METHODS

**2.1. TLC Method Development.** Developing a proper TLC method was important to be able to monitor the reactions. Most of these peroxides do not have a chromophore and do not reveal spots on UV or iodine. Moreover,  $\text{H}_2\text{SO}_4$  charring also proved unsuccessful. Finally, vanillin spray and basic  $\text{KMnO}_4$  solution revealed the spots.

**2.2. Spectroscopic Measurements.**  $^1\text{H}$  and  $^{13}\text{C}$  NMR spectra ( $\text{CDCl}_3$ ) were obtained on a Varian 300 MHz spectrometer (Varian Inc., Palo Alto, CA) in tubes with 5 mm exterior diameters. Depending on solubility, either  $\text{CDCl}_3$  or  $\text{DMSO-}d_6$  were used as a solvent. ESI-MS was recorded on a ThermoQuest, Finnigan LCQ-Duo instrument in positive ionization mode. FTIR analysis was performed using a Smart iTR ATR sampling accessory for a Nicolet iS10 spectrometer with a diamond crystal [Thermo Scientific, (Waltham, Massachusetts, USA)]. Comparison of the FTIR spectra of the resulting peroxides with the starting materials should reveal important information. The carbonyl peaks at  $\sim 1720\text{ cm}^{-1}$  should disappear for peroxides. We monitored the reactions similarly. ESI-MS was recorded on a ThermoQuest, Finnigan LCQ-Duo instrument coupled to an ESI source and to a Spectra System SCM 1000 gradient pump. The samples for analysis by ESI-MS were dissolved in methanol. Samples were introduced by injection through a  $5\ \mu\text{L}$  sample loop into a  $200\ \mu\text{L}/\text{min}$  flow of methanol/water (75:25) from the LC pump. Ammonium acetate was used as a preionization buffer. All measurement was Scanned for molecular ion peaks in positive ionization mode.

**2.3. DSC Measurements.** Samples ( $\sim 2\ \text{mg}$ ) were weighed by microanalytical balance  $\pm 1\ \mu\text{g}$ . The thermal behavior of the compounds was monitored using a DSC Q4000 (TA Instruments, New Castle, DE, USA). DSC thermograms were recorded by gradual heating from  $-25$  to  $250\ ^\circ\text{C}$  at a rate  $10\ ^\circ\text{C}/\text{min}$ . No preheating or cooling cycle was performed.

**2.4. Power Index: Evaluating Explosive Potentials through Systematic Analysis.** Detonation is a rapid, violent chemical reaction within a substance that propagates at supersonic speeds. It involves the almost instantaneous conversion of the substance into gases, accompanied by an intense release of energy. This reaction generates a shock wave that travels through the material, leading to its rapid decomposition.<sup>20</sup>

- Heat of Detonation.** The energy released during detonation is primarily in the form of heat, known as the heat of detonation ( $Q_{\text{det}}$ ), expressed in joules per gram or kilojoules per kilogram of the compound subjected to detonation. This measure assists in evaluating the potential of a compound to function as an energetic material. A higher heat of detonation signifies that more energy is released per unit mass, indicating a more potent explosive material.<sup>21</sup>
- Gas Volume.** The volume of gases ( $V_{\text{gas}}$ ) generated during detonation indicated of their potential for expansion work.<sup>22</sup> The gas volume released by each substance can be determined using eq 1:

$$V_{\text{gas}} = n_{\text{gas}} V_m \quad (1)$$

In this equation,  $n_{\text{gas}}$  signifies the number of moles of gases released during detonation.<sup>23</sup>

- Detonation Products and Oxygen Balance.** To determine the number of moles in the gaseous detonation products, it is essential to first identify the type of reaction taking place. The general formula of a potential energetic material is  $C_aH_bN_cO_dX_mM_m$ . In this formula, C, H, N, and O represent carbon, hydrogen, nitrogen, and oxygen, respectively. X signifies halogens while M denotes any metal (alkali, alkaline earth, or transition). The subscripts ( $a$ ,  $b$ ,  $c$ ,  $d$ ,  $x$ , and  $m$ ) indicate the respective quantities of these atoms within the formula compound.<sup>24</sup>

The Oxygen Balance (%OB) is used to assess the adequacy of oxygen atoms within a High Energy Material (HEM) to completely oxidize hydrogens into  $H_2O$  and carbons into  $CO_2$ . This measurement is calculated using eq 2:

$$\%OB = \frac{\left[ d - 2a - \frac{b}{2} \right] M(O)}{M(\text{HEM})} 100 \quad (2)$$

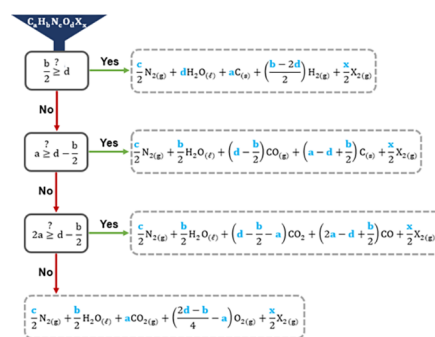
where  $d$ ,  $a$ , and  $b$  denote the quantities of oxygen, carbon, and hydrogen atoms within the HEM molecule.  $M(O)$  represents the molar mass of oxygen, while  $M(\text{HEM})$  signifies the molar mass of the specific High Energy Material under examination.<sup>23</sup>

During World War II, Kistiakowsky and Wilson formulated the K–W rules, a set of guidelines. These rules prioritize the conversion sequence during detonation: Initially, Carbon atoms shift to CO, followed by Hydrogen atoms converting to water. Any remaining Oxygen atoms trigger the conversion of CO to  $CO_2$ . It is crucial to emphasize that these guidelines are specifically designed for High Energetic Materials (HEMs) with %OB exceeding  $-40\%$ . In cases where %OB is less than  $-40\%$ , the modified Kistiakowsky–Wilson rules come into play. Scheme 1 facilitates the prediction of detonation reactions by analyzing the atomic composition of the compound, leveraging both Kistiakowsky–Wilson (K–W) original and modified rules.<sup>25–27</sup>

- Explosive power and Power Index.** The calculation of explosive power ( $P_e$ ), based on the heat and volume of gases released during detonation (eq 3), assesses a material's performance as a high-energetic material. The higher the value, the more energetic the compound.

$$P_e = Q_{\text{det}} V_{\text{gas}} \quad (3)$$

### Scheme 1. Predicting Detonation Reactions Based on K–W Rules



The Power Index (PI), represented by eq 4 in terms of percentage, serves as a comparative numerical metric used to assess the relative power of an explosive. This evaluation is based on the heat and volume of gases produced by the detonation of 1.0 g of the explosive material. In the systematic evaluation of High Energetic Materials (HEM) against standard explosives like picric acid (or TNT), the Power Index is computed as follows:

$$\begin{aligned} \%PI &= \frac{P_e(\text{HEM})}{P_e(\text{Picric acid})} 100 \\ &= \frac{Q_{\text{det}}(\text{HEM}) V_{\text{gas}}(\text{HEM})}{Q_{\text{det}}(\text{Picric acid}) V_{\text{gas}}(\text{Picric acid})} 100 \end{aligned} \quad (4)$$

Consistency is achieved by measuring the heat of detonation and gas volume for one gram of each substance. For example, detonating 1.0 g of picric acid releases 0.831 L of gas, with a reported heat of detonation value of 3250 J/g. This standardized approach ensures impartial and accurate comparisons, offering an unbiased assessment of explosive potentials.<sup>28,29</sup>

In our study, the heat of detonation for HEM was determined using DSC. Gas volume calculations were executed based on eq 1, following the prediction of products in accordance with the K–W rules.

**2.5. Screening of Cyclic Peroxides Using the ISE Model: A Computational Approach for Predictive Analysis.** Iterative Stochastic Elimination (ISE) algorithm is designed to create classification models specifically tailored to distinguish between active and inactive molecules. Good classification models enable a subsequent screening and scoring of any molecules by these models in order to predict their relevant properties. As an Artificial Intelligence technique, ISE learns from distinct activity variations observed within different molecular classes.

- Learning Set Construction.** The initial stage of building an ISE model involves constructing a learning set comprising both active and decoy molecules. This process encompasses several steps:

- Active Molecules.** Searching active molecules from literature or reliable sources. Subsequently, these molecules undergo structural standardization and calculation of some 206 2D MOE descriptors (molecular physicochemical properties), using MOE2018.<sup>30</sup> Based on these properties, an Applicability Domain (AD) is established.

- b. **Decoy Molecules.** After standardizing each molecule in the database and computing the same 206 2D MOE descriptors, the molecules underwent filtration via the AD. Decoy molecules (usually 100) were then randomly selected for each active molecule from the subset that passed this screening, maintaining a predetermined ratio.
- c. **Learning Set Formation.** The learning set is constructed within KNIME (version 2.10)<sup>31</sup> by combining *n* active molecules with decoys, resulting in a set comprising 101*n* molecules, each described by 206 2D descriptors. Descriptors showing constant values or high correlation (Pearson correlation coefficient >0.9) are excluded.
- 2 **ISE Model Construction.** The algorithm generates diverse filters by randomly selecting five ranges from a pool of 206 2D descriptors. These filters capture distinct physicochemical properties of molecules. Subsequently, the learning set undergoes screening through these filters, evaluating each filter's ability to discern between active molecules and decoys. Each filter's Matthews Correlation Coefficient (MCC) is calculated, ranging from -1 to 1, with 0 indicating random prediction. Filters with the lowest MCC values are iteratively removed until fewer than a million combinations remain. All filters are then ranked based on their MCC scores, from the highest to the lowest.
- 3 **ISE Model Evaluation via Cross-Validation.** This involves splitting the learning set randomly into 5 folds, each comprising 20% of the molecules while maintaining the ratio between active and inactive (decoy) molecules. Five "submodels" are generated, employing four folds for training and scoring the fifth fold, with each "submodel" using a different fold as the test set. The ISE algorithm processes the training set to create property-based filters. The test set for each "submodel" is screened through filters created by its respective training set, assigning positive scores to passing molecules and negative scores to failing ones. In the end of this process, all the learning set molecules receive scores, and filters were merged into a single model. During the model construction process, various criteria were employed to assess both the components of the model (e.g., MCC) and its overall quality (e.g., Precision, Accuracy, Recall, EF, ROC curve, and AUC-ROC).
- 4 **Database Screening and Activity Evaluation.** After model validation, the ISE model is used to filter any set of molecules, unlimited in size up to hundreds of millions, scoring molecules based on their assigned physicochemical properties and creating a molecular index (MI). Typically, we screen vast libraries containing millions of molecules, using a model to rank them and select the highest scoring ones for experimental validation. Each molecule received a Molecular Index (MI), assessing its predictive activity based on how well it passed through the model filters. The resulting MI ranges from -1 to +1, where a positive MI indicates activity, and a negative MI suggests inactivity. A higher MI signifies an elevated likelihood of experimental discovery as being active.<sup>32</sup> In our study, we focused on

analyzing 26 cyclic triperoxides that were synthesized in our laboratory.

Comprehensive descriptions elucidating the statistical and mathematical aspects of the ISE algorithm can be found.<sup>13,33</sup>

### 3. MATERIALS

All ketones were purchased from Sigma-Aldrich, Rosh HaAyin, Israel, and used as received. Two different concentrations of hydrogen peroxide solutions were used (30% and 50% in water), which were purchased from Sigma-Aldrich, Israel. All solvents were analytical-grade from Sigma-Aldrich (Rosh HaAyin, Israel) or BioLab (Jerusalem, Israel). They were used without further purification. The extraction solvents (pentane, diethyl ether, dichloromethane) were dried using anhydrous magnesium sulfate (BioLab, Jerusalem, Israel).

### 4. SYNTHESIS

We employed a uniform reaction condition for all compounds, following procedure 3 with a 2:1 H<sub>2</sub>O<sub>2</sub> ratio.<sup>34</sup> The reaction proceeded based on a specific molar ratio of ketone:H<sub>2</sub>O<sub>2</sub>:concentrated H<sub>2</sub>SO<sub>4</sub> at 1:2:0.3, utilizing both 50% and 30% H<sub>2</sub>O<sub>2</sub> concentrations. In a 5 mL screw-capped glass vial, 0.2 mL (or 0.2 g for solid ketones) of the ketone was added. Subsequently, 2 equiv of H<sub>2</sub>O<sub>2</sub> were introduced, and homogeneity achieved by the addition of 1 mL of THF. The reaction mixture was then cooled to below 0 °C using an ice-salt bath.

Concentrated H<sub>2</sub>SO<sub>4</sub> (0.3 equiv) was meticulously added dropwise to the cold mixture over a 10 min period. Stirring occurred for 2 h within an ice bath (~4–5 °C), followed by an overnight incubation (24 h) at room temperature. In instances where a clear, homogeneous solution was not attained, 1 mL of additional THF was added.

If immiscibility persisted, the mixture underwent 2 h of vigorous stirring on the ice bath, followed by vortexing for 5 min at 30 min intervals for 12 h. Subsequently, the mixture continued stirring at room temperature for an additional 12 h. Each tube underwent scrutiny after 24 h for any signs of separation. THF evaporation was executed using a nitrogen stream.

Any solid formed underwent separation through decantation and filtration, followed by a THF wash. Post-THF removal, 2 mL of pentane was added to each tube. The pentane layer was separated and dried with anhydrous magnesium sulfate. The aqueous layer underwent extraction with diethyl ether and dichloromethane, and the organic layer was subsequently dried using magnesium sulfate. Extracts from all samples underwent TLC using the solvent system, DCM:MeOH 90:10. Solvents underwent drying via a nitrogen stream, and resulting samples were weighed to report the crude yield.

Finally, to each reaction tube, 1 mL of ether was added and mixed thoroughly with Vortex for 1 min to facilitate separation.

### 5. RESULTS AND DISCUSSION

5.1. **TLC.** The TLC analyses revealed distinctive patterns for the postreaction products of ketones treated with varying concentrations of hydrogen peroxide. Acetone displayed a transition from a single spot at 30% to two spots at 50%, suggesting altered reaction pathways. Methyl ethyl ketone and isobutyl methyl ketone exhibited two spots at 30%, expanding to three spots at 50%, indicating potential multistage reactions. Notably, 4-heptanone showed three spots at 30%, reducing to

two at 50%, indicating a simplified reaction. In contrast, 2-heptanone maintained a consistent two-spot pattern, suggesting a stable reaction. Unfortunately, 3-pentanone exhibited no spots at 30% but three at 50%, indicating incomplete reactions or alternative pathways. Benzophenone displayed a consistent two-spot pattern at both 30% and 50% H<sub>2</sub>O<sub>2</sub> concentrations. Compounds, such as cyclohexanone, cyclopentanone and cycloheptanone, exhibited distinct TLC patterns between concentrations, emphasizing diverse reactivity patterns influenced by varying H<sub>2</sub>O<sub>2</sub> concentrations in the postreaction products.

**5.2. Spectroscopy.** **5.2.1. Acetone.** The FTIR analysis of the peroxide formed by combining acetone with 30% H<sub>2</sub>O<sub>2</sub> revealed the disappearance of peaks in 1711 and 900 cm<sup>-1</sup> associated with peroxides, indicating peroxide formation. Similar peak disappearance occurred with 50% H<sub>2</sub>O<sub>2</sub>, confirming peroxide formation. <sup>1</sup>H NMR analysis for both concentrations showed peaks at 1.5 ppm, confirming the presence of Triacetone Triperoxide (TATP). <sup>13</sup>C NMR identified a peak at 107 ppm, supporting the existence of the peroxide group (–C–O–O–) in line with TATP formation. ESI MS for acetone with 50% H<sub>2</sub>O<sub>2</sub> detected ions at 348 and 422 m/z, suggesting the presence of oligomeric peroxides. Collectively, FTIR, <sup>1</sup>H NMR, and ESI MS analyses confirmed TATP formation in both concentrations, with 50% H<sub>2</sub>O<sub>2</sub> resulting in more complex oligomeric peroxides.

**5.2.2. Methyl Ethyl Ketone (MEK).** For the product obtained from MEK using 30% H<sub>2</sub>O<sub>2</sub>, FTIR revealed the disappearance of characteristic peaks at approximately 1711 cm<sup>-1</sup>, 900 cm<sup>-1</sup> (indicative of O–O stretching), and a broad absorption band around 3200 cm<sup>-1</sup> (associated with –OH stretching). In the corresponding <sup>1</sup>H NMR spectrum, signals were detected at  $\delta = 1.1$  ppm (representing methyl groups, t, 6H) and  $\delta = 1.2–1.85$  ppm (indicating methylene groups, m). Upon employing 50% H<sub>2</sub>O<sub>2</sub>, similar FTIR and <sup>1</sup>H NMR results were obtained, displaying the disappearance of peaks around 1711 cm<sup>-1</sup>, 900 cm<sup>-1</sup>, and a broad band at 3200 cm<sup>-1</sup>. The NMR spectrum exhibited resonances at  $\delta = 1.1$  ppm (methyl groups, t, 6H) and  $\delta = 1.2–1.85$  ppm (methylene groups, m). Interestingly, in addition to these observations, Electrospray Ionization Mass Spectrometry (ESI MS) detected molecular ions at *m/z* 316, 404, 492, 580, 668, and 756, revealing the presence of oligomeric peroxides with the formula H(OOC(CH<sub>3</sub>)-CH<sub>2</sub>CH<sub>3</sub>)<sub>*n*</sub>OOH. Furthermore, ammonium ions with *n* values ranging from 3 to 8 were identified, suggesting varying degrees of polymerization. Notably, no significant observations were made in terms of conductivity in either the oligomeric peroxide or molecular ion tests for the 50% H<sub>2</sub>O<sub>2</sub> reaction products.

**5.2.3. Isobutyl Methyl Ketone.** Upon employing 30% H<sub>2</sub>O<sub>2</sub>, distinctive alterations were observed in the FTIR spectra of Isobutyl methyl ketone. Notably, the disappearance of the characteristic ketone carbonyl stretch (~1711 cm<sup>-1</sup>) suggested a significant chemical transformation involving the ketone moiety. Concurrently, new signals emerged around 900 cm<sup>-1</sup> (indicative of O–O stretching) and 3200 cm<sup>-1</sup> (a broad –OH stretch), implying the formation of oxygen-containing functional groups, likely peroxides, resulting from the interaction between the ketone and H<sub>2</sub>O<sub>2</sub>. Complementing these observations, the <sup>1</sup>H NMR analysis corroborated these structural changes by revealing distinctive shifts in the chemical shifts of hydrogen atoms. Specifically, peaks at  $\delta = 1.1$  ppm indicated the presence of methyl groups (–CH<sub>3</sub>, t, 6H), while a range between  $\delta = 1.2–1.85$  corresponded to methylene

(–CH<sub>2</sub>, m) protons, further supporting the formation of altered chemical entities arising from the reaction. Conversely, utilization of 50% H<sub>2</sub>O<sub>2</sub> primarily displayed observable changes in the FTIR and mass spectrometry analyses. Similar to the reaction with 30% H<sub>2</sub>O<sub>2</sub>, the disappearance of the ketone carbonyl stretch (~1711 cm<sup>-1</sup>) in the FTIR spectra indicated comparable reactivity, leading to the formation of oxygenated compounds. Furthermore, under 50% H<sub>2</sub>O<sub>2</sub> conditions, mass spectrometry (*m/z* in ESI MS) results revealed molecular ions exhibiting multiple peaks (285, 398, 516, 632, 748) consistent with the recurring formula H(OOC(CH<sub>3</sub>)CH<sub>2</sub>CH(CH<sub>3</sub>)<sub>2</sub>)<sub>*n*</sub>OOH. These ions, identified as ammonium adducts, showcased varying oligomerization states (*n* = 3, 4, 5, 6), indicating the formation of diverse oligomeric species resultant from the reaction.

**5.2.4. 4-Heptanone.** When subjected to 30% H<sub>2</sub>O<sub>2</sub>, 4-Heptanone exhibited incomplete reactivity. Subsequently, when subjected to a 50% concentration of H<sub>2</sub>O<sub>2</sub>, distinct observations emerged. Spectroscopic analysis revealed the disappearance of peaks around 1710 and 900 cm<sup>-1</sup>, indicating significant alterations in the chemical environment and the presence of an O–O stretching vibration, respectively. Further characterization via proton nuclear magnetic resonance ( $\delta = 1.5$  ppm) highlighted specific changes in the methyl (–CH<sub>3</sub>) group, involving 6 hydrogen atoms. Electrospray ionization mass spectrometry (ESI MS) showcased distinctive peaks at *m/z* 312, 442, 572, and 702, signifying the formation of H(OOC(CH<sub>2</sub>CH<sub>3</sub>)<sub>2</sub>)<sub>*n*</sub>OOH species, with *n* values ranging from 2 to 5. Notably, NH<sub>4</sub><sup>+</sup> ions were not observed.

**5.2.5. 2-Heptanone.** The reaction employing 30% H<sub>2</sub>O<sub>2</sub> with 2-Heptanone was notably incomplete. In experiments employing 50% H<sub>2</sub>O<sub>2</sub>, the FTIR analysis revealed the disappearance of characteristic peaks at approximately 1715 and 900 cm<sup>-1</sup>, attributed to the stretching vibrations of O–O bonds, suggesting substantial consumption of peroxide species. Simultaneously, the <sup>1</sup>H NMR spectrum exhibited a distinct signal at  $\delta = 1.5$  ppm, corresponding to six equivalent methyl protons (–CH<sub>3</sub>) within the 2-Heptanone structure. Furthermore, the analysis of oligomeric peroxides via ESI MS yielded molecular ions at *m/z* (ESI MS) 441, 571, and 701. These ions were tentatively assigned to H(OOC(CH<sub>3</sub>)-(CH<sub>2</sub>)<sub>4</sub>(CH<sub>3</sub>)<sub>4</sub>OOH and NH<sub>4</sub><sup>+</sup> species, indicating various degrees of oligomerization (*n* = 3, 4, 5). No molecular ions directly correlated to the initial 2-Heptanone starting material were detected in the mass spectra.

**5.2.6. 3-Pentanone.** Under different H<sub>2</sub>O<sub>2</sub> concentrations, distinct reactions were observed in the study involving 3-Pentanone. While the use of a 30% H<sub>2</sub>O<sub>2</sub> concentration resulted in an incomplete reaction, the employment of a 50% H<sub>2</sub>O<sub>2</sub> concentration yielded significant variations in product outcomes. Analysis through FTIR spectroscopy demonstrated the disappearance of characteristic peaks at approximately 1713 and 900 cm<sup>-1</sup>, attributed to the stretching vibrations associated with O–O bonds in peroxides. Simultaneously, <sup>1</sup>H NMR spectroscopy revealed signals at  $\delta = 1.5$  ppm, indicative of the presence of methyl groups (–CH<sub>3</sub>, 6H) within the resulting product. Intriguingly, mass spectrometry (ESI MS) unveiled molecular ions at *m/z* 358, 460, and 562, corresponding to a complex oligomeric peroxide identified as H(OOC(CH<sub>3</sub>CH<sub>2</sub>)<sub>2</sub>)<sub>5</sub>OOH. These ions were found in conjunction with NH<sub>4</sub><sup>+</sup> at diverse oligomeric states (*n* = 3, 4, 5). Notably, molecular ions representative of the original 3-Pentanone were conspicuously absent in the mass spectra.

**5.2.7. Cyclohexanone.** In both instances (30% and 50% H<sub>2</sub>O<sub>2</sub>), the FTIR spectra of the Cyclohexanone's products exhibited a disappearance of characteristic peaks around 1705 and 900 cm<sup>-1</sup>, indicative of O–O stretching vibrations typical of peroxide formation. Concurrently, the <sup>1</sup>H NMR spectra showcased signals consistent with Cyclohexane in the range of  $\delta = 1.2\text{--}1.9$  ppm for both 30% and 50% H<sub>2</sub>O<sub>2</sub> concentrations, affirming the retention of the cyclohexane moiety. In 50% H<sub>2</sub>O<sub>2</sub> concentration, a multiple molecular ions were detected by ESI MS analysis at  $m/z$  352, 452, and 552, correlating with H(OOC(CH<sub>2</sub>)<sub>4</sub>)<sub>n</sub>OOH species, indicating oligomerization. Further, the presence of NH<sub>4</sub><sup>+</sup> ions suggested varying oligomeric sizes, specifically  $n = 3, 4,$  and  $5$  within these structures. Additionally, the ESI MS unveiled a spectrum of molecular ions, including  $m/z$  229 (dimer), 247 (dimer + NH<sub>4</sub><sup>+</sup>), 264 (dimer + 2 NH<sub>4</sub><sup>+</sup>),  $m/z$  343 (trimer), 360 (trimer + NH<sub>4</sub><sup>+</sup>), and 378 (trimer + 2 NH<sub>4</sub><sup>+</sup>), illustrating the complexity and diversity of the oligomeric peroxide compositions at this higher concentration.

**5.2.8. Cyclopentanone.** The spectroscopic analysis of the reaction product resulting from the interaction between Cyclopentanone and 30% H<sub>2</sub>O<sub>2</sub> reveals significant changes in its chemical composition. The FTIR spectra display the disappearance of characteristic peaks around 1705 and 900 cm<sup>-1</sup>, indicative of O–O stretching vibrations associated with peroxide formation. Concurrently, the <sup>1</sup>H NMR spectra demonstrate signals consistent with Cyclopentane in the range of  $\delta = 1.4\text{--}1.8$  ppm, confirming the retention of the cyclopentane moiety. These findings are consistent with the formation of cyclic peroxides. Upon utilizing a higher concentration of H<sub>2</sub>O<sub>2</sub> (50%), the reaction product's spectroscopic profile undergoes notable changes. The FTIR spectra exhibit the disappearance of peaks around 1742 and 900 cm<sup>-1</sup>, indicating O–O stretching vibrations characteristic of peroxide formation. The <sup>1</sup>H NMR spectra continue to reveal signals consistent with Cyclopentane in the range of  $\delta = 1.4\text{--}1.8$  ppm, affirming the preservation of the cyclopentane structure. The ESI MS analysis detects multiple molecular ions at  $m/z$  352, 452, and 552, corresponding to H(OOC(CH<sub>2</sub>)<sub>4</sub>)<sub>n</sub>OOH species, indicative of oligomerization. The presence of NH<sub>4</sub><sup>+</sup> ions suggests varying oligomeric sizes, specifically  $n = 3, 4,$  and  $5$  within these structures. Further complexity is unveiled through the ESI MS spectra, which display molecular ions at  $m/z$  201 (dimer), 219 (dimer + NH<sub>4</sub><sup>+</sup>), 301 (trimer), 319 (trimer + NH<sub>4</sub><sup>+</sup>), and 336 (trimer + 2 NH<sub>4</sub><sup>+</sup>). However, no significant change is observed using 50% H<sub>2</sub>O<sub>2</sub>.

**5.2.9. Cycloheptanone.** At 30% H<sub>2</sub>O<sub>2</sub> concentration, the FTIR and NMR data suggest an incomplete reaction, as specific peaks or signals indicative of peroxide formation are not observed. However, at 50% H<sub>2</sub>O<sub>2</sub> concentration, significant changes are evident in the spectroscopic profile. The FTIR spectra display the disappearance of peaks around 1698 and 900 cm<sup>-1</sup>, characteristic of O–O stretching vibrations associated with peroxide formation. Simultaneously, the <sup>1</sup>H NMR spectra reveal signals at  $\delta = 1.5$  ppm, corresponding to the methyl groups (–CH<sub>3</sub>) of Cycloheptane, indicating the presence of cyclic peroxide. This is further supported by spectral analysis, confirming the formation of cyclic peroxides.

**5.2.10. Hexafluoroacetone.** At both 30% and 50% H<sub>2</sub>O<sub>2</sub> concentrations, the FTIR spectra display the disappearance of peaks around 1626 cm<sup>-1</sup>, indicating the presence of O–O

stretching vibrations characteristic of peroxide formation. Spectral analysis confirms the formation of peroxides. The disappearance of the 1626 cm<sup>-1</sup> peak suggests the involvement of Hexafluoroacetone in peroxide formation.

**5.3. DSC.** TATP, a prevalent cyclic peroxide in improvised explosives, has well-documented detonation heat values ranging from 2454 to 2896 J/g, contingent on the heating rate, with the higher rate correlating to a lower energy release.<sup>35</sup> In our research the heat flow was 10 °C

**5.3.1. Acetone.** Distinct thermal behaviors were observed for Acetone-derived cyclic peroxide at 30% and 50% H<sub>2</sub>O<sub>2</sub> concentrations. At 30%, a single exothermic peak at 69.76 °C, with a heat flow of 2597.49 J/g, indicated a straightforward reaction. At 50%, two peaks (65 and 108 °C) suggested a more intricate decomposition, with the second peak exhibiting significantly increased energy release (1640.96 J/g). The higher concentration facilitated the formation of diverse reaction products, leading to a different decomposition pathway.

**5.3.2. Methyl Ethyl Ketone (MEK).** MEK-derived cyclic peroxide exhibits concentration dependent reactivity with hydrogen peroxide (H<sub>2</sub>O<sub>2</sub>). At 30%, no discernible detonation temperature or heat flow was observed. In contrast, at 50%, a detonation temperature of 169.73 °C and heat flow of 589.00 J/g, coupled with broad peaks from 122.6 to 193 °C, indicate a complex decomposition process with diverse reaction products. This concentration-dependent difference underscores the reaction's sensitivity, with 50% H<sub>2</sub>O<sub>2</sub> leading to a more energetic and complex decomposition compared to the minimal reactivity observed at 30%.

**5.3.3. Isobutyl Methyl Ketone.** At 30%, the resulting cyclic peroxide exhibits complex decomposition, evidenced by two broad exothermic peaks (87–198 °C) with shoulders at 87–155 °C and 155–198 °C. Heat flows of 935.78 J/g and 256.44 J/g suggest involvement of multiple reaction steps or various reaction products. At 50%, the cyclic peroxide displays a well-defined exothermic peak at 186.97 °C, with a broad profile (116.6–225 °C) and merged shoulders. The associated heat flow of 1275.27 J/g indicates a more substantial energy release during detonation compared to the 30% concentration, suggesting a more intricate and energetically favorable process. This highlights concentration-dependent variations in detonation behavior and energy release, attributed to diverse reaction pathways and product formations.

**5.3.4. 4-Heptanone.** At 30%, the cyclic peroxide displayed a detonation temperature of 126.97 °C, accompanied by a heat flow of 579.43 J/g. Two merged exothermic peaks were observed, with one dominant peak covering approximately 80% of the reaction from 95 to 155 °C, and a secondary, extremely small peak observed from 155 to 181 °C. This intricate thermal profile suggests a nuanced decomposition process, potentially involving multiple reaction steps or the formation of various reaction products. At 50%, the cyclic peroxide exhibited a detonation temperature of 140.67 °C, with a substantially increased heat flow of 1342.61 J/g. A broad and single exothermic peak ranging from 100 to 166 °C was observed, indicating a more homogeneous explosive decomposition process.

**5.3.5. 2-Heptanone.** Here, the cyclic organic peroxide product demonstrated a detonation temperature of 142.92 °C at 30%, accompanied by a heat flow of 672.64 J/g. A broad and singular exothermic peak, ranging from 105 to 159 °C, was observed, suggesting a relatively uniform explosive decom-

position process. Upon increasing the concentration to 50%, the cyclic peroxide exhibited a higher detonation temperature of 149.88 °C, along with an elevated heat flow of 1001.56 J/g. Here, a broad single exothermic peak ranging from 108 to 171 °C was observed, indicating a more energetically favorable explosive decomposition process at the higher concentration.

**5.3.6. 3-Pentanone.** At 30%, the detonation temperature and heat flow were not determined. However, at 50%, the cyclic peroxide exhibited a detonation temperature of 187.45 °C, accompanied by a heat flow of 990.31 J/g. The thermal profile revealed broad exothermic peaks ranging from 110 to 230 °C, with two merged shoulders. The first shoulder spanned approximately 110–165 °C, and the second 165–230 °C. This complex thermal signature suggests a diverse and energetic explosive decomposition process at the higher concentration.

**5.3.7. Cyclohexanone.** At 30%, the cyclic peroxide displayed a detonation temperature of 131.02 °C, accompanied by a heat flow of 884.21 J/g. A broad and singular exothermic peak ranging from 101 to 159 °C was observed, indicating a relatively uniform and moderate explosive decomposition process. In contrast, at 50%, the cyclic peroxide exhibited a detonation temperature of 99.04 °C, with a significantly increased heat flow of 2342.72 J/g. The thermal profile revealed extremely broad exothermic peaks ranging from 58.6 to 191 °C, with two shoulders merged. One shoulder spanned approximately 60–120 °C, and the other 120–190 °C. This intricate thermal behavior suggests a more complex and energetically favorable explosive decomposition process at the higher concentration.

**5.3.8. Cyclopentanone.** The thermal analysis conducted on the peroxidic cyclic organic product derived from the reaction between Cyclopentanone and hydrogen peroxide at two concentrations (30% and 50%) revealed concentration-dependent variations in detonation temperature and heat flow. At 30%, the cyclic peroxide displayed a high detonation temperature of 185.95 °C, coupled with a substantial heat flow of 1462.55 J/g. The thermal profile exhibited a sharp and singular exothermic peak, suggesting a focused and energetically robust explosive decomposition process. Conversely, at 50%, the cyclic peroxide exhibited a lower detonation temperature of 96.04 °C, with a decreased heat flow of 893.87 J/g. Nevertheless, a sharp and singular exothermic peak was observed, indicating a distinctive yet energetically favorable explosive decomposition process at the higher concentration.

The presence of sharp, single exothermic peaks at both 30% and 50% concentrations implies a simplified and efficient decomposition, potentially resulting in a more uniform reaction product.

**5.3.9. Cycloheptanone.** Unfortunately, at 30%, reaction incomplete. However, at 50%, the cyclic peroxide exhibited a detonation temperature of 179.27 °C, accompanied by a substantial heat flow of 1889.32 J/g. The thermal profile displayed extremely broad exothermic peaks ranging from 51 to 203 °C, with two shoulders merged. The first, smaller shoulder spanned approximately 51–100 °C, while the second, more pronounced shoulder, covered the range of 100–203 °C.

**5.3.10. Hexafluoroacetone.** At both 30% and 50% H<sub>2</sub>O<sub>2</sub> concentrations, the product obtained from the reaction between H<sub>2</sub>O<sub>2</sub> and Hexafluoroacetone, exhibited no exothermic peaks in the DSC tests.

Most TCPs exhibited exothermic behavior. Detonation, characterized by the rapid propagation of a shockwave through a material and an immediate energy release, is typically illustrated as a sharp, singular exothermic peak in a DSC curve - similar to what is observed in the DSC results for TCP8.

**5.4. Power Index.** Under our experimental conditions, the primary expected peroxide is the trimeric cyclic compound. We calculated the %OB for each trimeric cyclic peroxide (TCP) based on its atomic composition and eq 2. Table 1 displays the structures of 10 ketones along with their corresponding trimeric cyclic peroxides (TCP) and their respective %OB values

All trimeric cyclic peroxides (TCPs) exhibited oxygen balance values below -40%. In these instances, anticipated reactions were determined following the K–W modified rules. Table 2 presents the predicted detonation reactions for each TCP, as per Scheme 1.

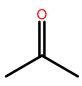
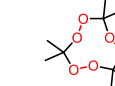
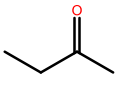
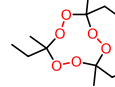
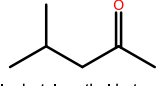
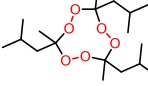
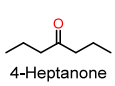
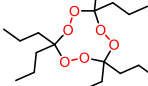
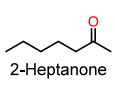
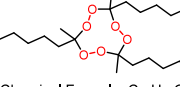
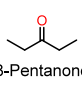
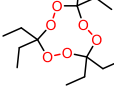
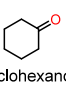
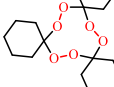
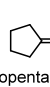
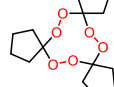
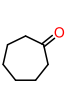
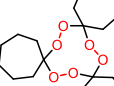
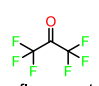
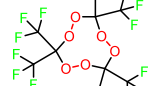
As outlined in the introduction, it is crucial to elucidate the nature of the detonation process for calculating a power index. Gas moles are precisely computed per 1.0 g of TCP, considering the specific detonation reaction type. The heat of detonation is determined from our conducted DSC measurements. In instances where multiple exothermic peaks were observed for the TCP, the most exothermic peak was selected for calculation purposes. Gas volumes were computed using eq 1, where the molar volume is set at standard temperature and pressure (STP) conditions (22.40 L/mol). It is important to note that the molar volume ( $V_m$ ) is responsive to variations in temperature and pressure. However, since the molar volume is calculated for both the potential energetic substance and the standard energetic substance (picric acid in our case) in eq 4 as a ratio, the specific value of the molar volume becomes inconsequential as long as it remains consistent for both substances. Due to the elevated temperature of the detonation reaction, all resulting products are in gaseous form, with the exception of carbon, which remains in a solid state.

Consequently, a power index was derived for each TCP using eq 4. The findings are detailed in Table 3.

The Power Index (%PI) reflects the efficiency of energy transfer from the explosive material to the surrounding environment. Higher %PI values suggest more efficient energy transfer, making the compound more potent in terms of explosive power. As anticipated, TATP demonstrates a high %PI. Notably, TCP07 exhibits a %PI very close to that of TATP (86% and 88%, respectively).

**5.5. ISE Model. 5.5.1. Constructing Learning Set.** The ISE Model was constructed on the basis of 202 HEMs obtained from various sources.<sup>36–39</sup> Duplicates were removed based on their similarity (Tanimoto Index), using Chemistry Development Kit (CDK) nodes<sup>40</sup> integrated within the KNIME (version 2.10) platform.<sup>31</sup> The Applicability Domain (AD) encompasses five key descriptors: the count of carbon, nitrogen, oxygen atoms, and molecular weight. The determination of these domain descriptors relied on essential parameters necessary for computing the oxygen balance of energetic molecules and determining the volume of gases released during its detonation reaction. The boundaries for each of the five descriptors were established by considering the mean plus standard deviation of these features, calculated for all the 202 active molecules. Decoy molecules from the Enamine database (~2 million molecules)<sup>41</sup> were selectively chosen within the AD to be part of the learning set.

**Table 1. Structures of Ketones, Corresponding TCP, and % OB Values**

TCP	Ketone Origin Structure	TCP Structure	%OB (TCP)
TCP1	 Acetone	 Chemical Formula: C <sub>9</sub> H <sub>18</sub> O <sub>6</sub>	-151
TCP2	 Methyl ethyl ketone	 Chemical Formula: C <sub>12</sub> H <sub>24</sub> O <sub>6</sub>	-182
TCP3	 Isobutyl methyl ketone	 Chemical Formula: C <sub>18</sub> H <sub>36</sub> O <sub>6</sub>	-220
TCP4	 4-Heptanone	 Chemical Formula: C <sub>21</sub> H <sub>42</sub> O <sub>6</sub>	-233
TCP5	 2-Heptanone	 Chemical Formula: C <sub>21</sub> H <sub>42</sub> O <sub>6</sub>	-266
TCP6	 3-Pentanone	 Chemical Formula: C <sub>15</sub> H <sub>30</sub> O <sub>6</sub>	-204
TCP7	 Cyclohexanone	 Chemical Formula: C <sub>18</sub> H <sub>30</sub> O <sub>6</sub>	-210
TCP8	 Cyclopentanone	 Chemical Formula: C <sub>15</sub> H <sub>24</sub> O <sub>6</sub>	-192
TCP9	 Cycloheptanone	 Chemical Formula: C <sub>21</sub> H <sub>36</sub> O <sub>6</sub>	-233
TCP10	 Hexafluoroacetone	 Chemical Formula: C <sub>9</sub> F <sub>18</sub> O <sub>6</sub>	-94

**Table 2. Predicted Detonation Reactions for TCP Based on K–W Rules**

TCP	Detonation Reaction
TCP1	C <sub>9</sub> H <sub>18</sub> O <sub>6(s)</sub> → 6H <sub>2</sub> O <sub>(l)</sub> + 9C <sub>(s)</sub> + 3H <sub>2(g)</sub>
TCP2	C <sub>12</sub> H <sub>24</sub> O <sub>6(s)</sub> → 6H <sub>2</sub> O <sub>(l)</sub> + 12C <sub>(s)</sub> + 6H <sub>2(g)</sub>
TCP3	C <sub>18</sub> H <sub>36</sub> O <sub>6(s)</sub> → 6H <sub>2</sub> O <sub>(l)</sub> + 18C <sub>(s)</sub> + 12H <sub>2(g)</sub>
TCP4	C <sub>21</sub> H <sub>42</sub> O <sub>6(s)</sub> → 6H <sub>2</sub> O <sub>(l)</sub> + 33C <sub>(s)</sub> + 27H <sub>2(g)</sub>
TCP5	C <sub>33</sub> H <sub>66</sub> O <sub>6(s)</sub> → 6H <sub>2</sub> O <sub>(l)</sub> + 33C <sub>(s)</sub> + 27H <sub>2(g)</sub>
TCP6	C <sub>15</sub> H <sub>30</sub> O <sub>6(s)</sub> → 6H <sub>2</sub> O <sub>(l)</sub> + 15C <sub>(s)</sub> + 9H <sub>2(g)</sub>
TCP7	C <sub>18</sub> H <sub>30</sub> O <sub>6(s)</sub> → 6H <sub>2</sub> O <sub>(l)</sub> + 18C <sub>(s)</sub> + 9H <sub>2(g)</sub>
TCP8	C <sub>15</sub> H <sub>24</sub> O <sub>6(s)</sub> → 6H <sub>2</sub> O <sub>(l)</sub> + 15C <sub>(s)</sub> + 6H <sub>2(g)</sub>
TCP9	C <sub>23</sub> H <sub>40</sub> O <sub>6(s)</sub> → 6H <sub>2</sub> O <sub>(l)</sub> + 23C <sub>(s)</sub> + 14H <sub>2(g)</sub>
TCP10	C <sub>9</sub> F <sub>18</sub> O <sub>6(s)</sub> → 6CO <sub>(g)</sub> + 3C <sub>(s)</sub> + 9F <sub>2(g)</sub>

**Table 3. Detonation Performance Metrics for TCPs**

TCP	n(gas) (mol)	V(gas) (L)	Q(J/g)	%PI
TCP1	0.041	0.918	2597	88
TCP2	0.045	1.008	589	22
TCP3	0.052	1.165	1275	55
TCP4	0.054	1.210	1343	60
TCP5	0.059	1.322	1002	49
TCP6	0.049	1.098	990	40
TCP7	0.044	0.986	2342	86
TCP8	0.040	0.896	1463	49
TCP9	0.048	1.075	1889	75
TCP10	0.103	2.307	0	0

Maintaining a ratio of 1:100 between active molecules and decoys, the learning set of the model comprised 202 active molecules and 20,200 decoys.

**5.5.2. Model Evaluation.** Table 4 presents the minimum, maximum, and mean values of MCC, along with the AUC-

**Table 4. Filter Counts, MCC Scores, and AUC across Five Folds**

Fold	MCC Range	AUC-ROC	No. of Filters
1	0.75–0.83	0.99	590
2	0.74–0.82	0.98	577
3	0.76–0.83	0.96	486
4	0.76–0.82	0.99	484
5	0.76–0.84	0.97	603

ROC scores, for the five folds. The observed stability in MCC scores and the consistently high AUC-ROC values underscore the reliability of our set of filters. These findings suggest that our model exhibits robust performance across different test scenarios, affirming its potential utility in accurately identifying HEMs. Thus, it calls for combining the results of the folds—the filters that have been created in each are combined.

The ROC curve analysis of the model reveals a high AUC-ROC value of 0.98, emphasizing the model's robustness in accurately capturing the true positive rate while minimizing false positives. This strong discriminatory capacity underscores the model's effectiveness in identifying HEMs within the data set.

Table 5 displays the Confusion Matrix (CM) values at different cutoff indexes, accompanied by computed metrics such as True Positive Rate (TPR), False Positive Rate (FPR), and Enrichment Factor (EF).



**Table 5. Values of the Confusion Matrix (CM) at Different Cutoff Indexes**

	TP	FP	FN	TN	TPR	FPR	EF
Index 0	177	825	25	19375	0.88	0.04	18
Index 0.1	168	699	34	19501	0.83	0.03	20
Index 0.2	164	592	38	19608	0.81	0.03	22
Index 0.3	156	465	46	19735	0.77	0.02	25
Index 0.4	147	360	55	19840	0.73	0.02	29
Index 0.5	139	304	63	19896	0.69	0.02	32
Index 0.6	135	296	67	19904	0.67	0.01	32
Index 0.7	127	207	75	19993	0.63	0.01	38
Index 0.8	106	121	96	20079	0.52	0.01	47
Index 0.9	0	0	202	20200	0	0	
Index 1	0	0	202	20200	0	0	

The TPR, FPR and EF were calculated by

$$\text{TPR} = \frac{\text{TP}}{\text{TP} + \text{FN}} \quad (5)$$

$$\text{FPR} = \frac{\text{FP}}{\text{FP} + \text{TN}} \quad (6)$$

$$\text{EF} = \frac{\text{TP}/(\text{TP} + \text{FP})}{(\text{TP} + \text{FN})/(\text{TP} + \text{TN} + \text{FP} + \text{FN})} \quad (7)$$

These metrics offer a comprehensive view of the model's performance across various threshold settings.

We calculated 206 Molecular MOE descriptors for each of the 10 trimeric cyclic compound. Subsequently, we scored each molecule using our developed ISE model. Table 6 presents their corresponding ISE scores.

**Table 6. ISE Scores of TCPs**

TCP	ISE Score
TCP1	0.76
TCP2	0.70
TCP3	0.70
TCP4	0.70
TCP5	0.70
TCP6	0.26
TCP7	0.72
TCP8	0.64
TCP9	0.70
TCP10	0.21

The combined results from experimental assessments (%PI) and computational analyses (ISE Score) provide valuable insights into the energetic potential of synthesized cyclo-peroxide compounds (TCPs). Notably, TCP1, identified as TATP, demonstrated the highest values in both %PI calculation (88%) and ISE score (0.76), with TCP7 exhibiting the second-highest %PI (86%) and ISE score (0.72), reinforcing consistency between experimental and computational data. Additionally, TCP3, TCP4, and TCP8 displayed %PI values of 55%, 60%, and 49%, respectively, aligning closely with their corresponding ISE scores of 0.7. Conversely, TCP10 exhibited minimal energetic potential with a %PI of 0% and an ISE score of 0.21, while TCP6 showed a %PI of 40% alongside an ISE score of 0.26. TCP8 stood out with higher %PI and ISE scores compared to TCP6 and TCP10, indicative of its increased energetic activity. However, a discrepancy arose with

TCP2, which displayed a %PI of 22% despite consistently high ISE scores of 0.7, suggesting that certain experimental factors influencing %PI may not be fully captured by the computational model. We conducted a Pearson correlation analysis to examine the relationship between ISE Score and %PI. The correlation coefficient yielded a strong positive correlation of 0.691 ( $p = 0.027$ ), indicating a significant association between the two variables at the 0.05 level (2-tailed).

The agreement between experimental and computational results underscores the reliability of the ISE model in identifying energetic compounds. While the model effectively discerned TCPs with low %PI values (TCP6, TCP10), the misclassification of TCP2 highlights the need for further refinement and consideration of additional experimental variables in computational predictions. Furthermore, the study emphasizes the efficacy of the ISE model as a valuable tool for predicting the energetic nature of cyclo-peroxide compounds. This computational approach proves to be a time-saving and cost-effective preliminary screening tool, guiding attention toward compounds with the highest predicted scores for subsequent experimental examination.

Out of the 202 active molecules in the learning set, 22 are peroxides. Calculating the degree of molecular similarity (Tanimoto index) between the 10 molecules (TCP1 to TCP10) scored by the model and these 22 molecules, it was found that the highest Tanimoto index is 0.77, the lowest is 0.07, and the overall average is 0.24. These values suggest a very low degree of molecular similarity between a group of molecules in the learning set and the molecules synthesized and tested. Therefore, our ISE model may be used also to suggest synthesis of new cyclic peroxides that could have different energy releasing abilities.

## 6. CONCLUSIONS

The synthesis of new energetic materials involves a meticulous process, necessitates the use of various resources, and requires safety considerations. This manuscript underscores the viability of employing a computational pathway, specifically utilizing the ISE model.

In this study, new cyclo-peroxide compounds (CPs) were synthesized by reacting 13 different ketones with two concentrations of H<sub>2</sub>O<sub>2</sub>. Following spectroscopic analysis, we narrowed down our new compounds to 10, on which we conducted calorimetric tests. Utilizing the calorimetric results and K–W modified rules, we calculated %PI for these compounds.

An ISE model was constructed, and the statistical metrics results suggest that this model exhibits strong predictive abilities. We then screened the new CPs through the model filters, assigning each molecule a score based on its success in passing the model's filters.

Comparing the %PI obtained from the experimental approach to the ISE index derived from the computational approach led to the conclusion that both methods yield similar assessments regarding the potential of a new compound as an energetic material. Our research suggests that this observation holds true, especially in the context of synthesizing new cyclic peroxides. Consequently, it is indicated that, at least for cyclic peroxidic compounds, utilizing the ISE model is preferable for predicting the potential of a new compound to be an energetic substance. By employing the ISE model, similar conclusions can be reached in a faster, more cost-effective, and safer

manner, ensuring that only new compounds with the highest ISE scores undergo experimental examination.

Further investigation into ester nitrates can be intriguing, utilizing both experimental (synthesis, spectroscopy, and DSC) and computational approaches by scoring potential high-energy compounds with the ISE model.

## AUTHOR INFORMATION

### Corresponding Author

Abraham J. Domb – *The Institute for Drug Research, School of Pharmacy, Faculty of Medicine, The Hebrew University of Jerusalem, Jerusalem 91905, Israel*; [orcid.org/0000-0002-2241-7726](https://orcid.org/0000-0002-2241-7726); Email: [avid@ekmd.huji.ac.il](mailto:avid@ekmd.huji.ac.il)

### Authors

Mazal Rachamim – *Molecular Modelling and Drug Design Lab, Institute for Drug Research and Fraunhofer Project Center for Drug Discovery and Delivery, Faculty of Medicine, The Hebrew University of Jerusalem, Jerusalem 91905, Israel*; [orcid.org/0000-0001-8093-832X](https://orcid.org/0000-0001-8093-832X)

Amiram Goldblum – *Molecular Modelling and Drug Design Lab, Institute for Drug Research and Fraunhofer Project Center for Drug Discovery and Delivery, Faculty of Medicine, The Hebrew University of Jerusalem, Jerusalem 91905, Israel*

Complete contact information is available at:

<https://pubs.acs.org/10.1021/acsomega.4c03672>

### Notes

The authors declare no competing financial interest.

## REFERENCES

- (1) Zapata, F.; García-Ruiz, C. Chemical classification of explosives. *Critical Reviews in Analytical Chemistry* **2021**, *51* (7), 656–673.
- (2) Klapötke, T. M. Chemistry of High-Energy Materials. In *Chemistry of High-Energy Materials*; De Gruyter, 2017.
- (3) Peña-Quevedo, A. J.; Laramee, J. A.; Durst, H. D.; Hernández-Rivera, S. P. Cyclic organic peroxides characterization by mass spectrometry and raman microscopy. *IEEE Sensors Journal* **2011**, *11* (4), 1053–1060.
- (4) Keshavarz, M. H.; Klapötke, T. M. Energetic Compounds. In *Energetic Compounds*; de Gruyter, 2020.
- (5) Yuan, W. L.; He, L.; Tao, G. H.; Shreeve, J. N. M. Materials-Genome Approach to Energetic Materials. *Accounts of Materials Research* **2021**, *2* (9), 692–696.
- (6) Davis, T. L. *The Chemistry of Powder and Explosives*; Pickle Partners Publishing, 2016.
- (7) Türker, L. Peroxide Based Organic Explosives. *Earthline Journal of Chemical Sciences* **2021**, *6* (2), 165–208.
- (8) Klappec, D. J.; Czarnopys, G.; Pannuto, J. Interpol review of detection and characterization of explosives and explosives residues 2016–2019. *Forensic science international: Synergy* **2020**, *2*, 670–700.
- (9) Zhang, T.; Hu, X.; Zu, B.; Dou, X. A March to Shape Optical Artificial Olfactory System toward Ultrasensitive Detection of Improvised Explosives. *Advanced Photonics Research* **2022**, *3*, No. 2200006.
- (10) Evans, H. K.; Rasmussen, C. A.; Tulleners, F. A. J.; Sanchez, B. L. An unusual explosive, triacetoneperoxide (TATP). *Journal of Forensic Sciences* **1986**, *31* (3), 1119–1125.
- (11) Matyáš, R.; Pachman, J. Study of TATP: Influence of reaction conditions on product composition. *Propellants, Explosives, Pyrotechnics: An International Journal Dealing with Scientific and Technological Aspects of Energetic Materials* **2010**, *35* (1), 31–37.
- (12) Rarata, G.; Vahčić, M.; Anderson, D.; Berglund, M.; Kyprianou, D.; Emma, G.; Diaconu, G. Hydrogen peroxide (H<sub>2</sub>O<sub>2</sub>): a review of its use in homemade explosives. *Materiały Wysokoenergetyczne* **2019**, *11* (2), 5–13.
- (13) Stern, N.; Goldblum, A. Iterative stochastic elimination for solving complex combinatorial problems in drug discovery. *Isr. J. Chem.* **2014**, *54* (8–9), 1338–1357.
- (14) Cern, A.; Marcus, D.; Tropsha, A.; Barenholz, Y.; Goldblum, A. New drug candidates for liposomal delivery identified by computer modeling of liposomes' remote loading and leakage. *J. Controlled Release* **2017**, *252*, 18–27.
- (15) Da'adoosh, B.; Marcus, D.; Rayan, A.; King, F.; Che, J.; Goldblum, A. Discovering highly selective and diverse PPAR-delta agonists by ligand based machine learning and structural modeling. *Sci. Rep.* **2019**, *9* (1), 1–12.
- (16) El-Atawneh, S.; Hirsch, S.; Hadar, R.; Tam, J.; Goldblum, A. Prediction and experimental confirmation of novel peripheral cannabinoid-1 receptor antagonists. *J. Chem. Inf. Model.* **2019**, *59* (9), 3996–4006.
- (17) Da'adoosh, B.; Kaito, K.; Miyashita, K.; Sakaguchi, M.; Goldblum, A. Computational design of substrate selective inhibition. *PLoS computational biology* **2020**, *16* (3), No. e1007713.
- (18) El-Atawneh, S.; Goldblum, A. Candidate Therapeutics by Screening for Multitargeting Ligands: Combining the CB2 Receptor With CB1, PPAR $\gamma$  and 5-HT4 Receptors. *Front. Pharmacol.* **2022**, *13*, DOI: 10.3389/fphar.2022.812745.
- (19) Wolk, O.; Goldblum, A. Predicting the Likelihood of Molecules to Act as Modulators of Protein–Protein Interactions. *J. Chem. Inf. Model.* **2023**, *63* (1), 126–137.
- (20) Zhang, Z. X. *Rock Fracture and Blasting: Theory and Applications*; Butterworth-Heinemann, 2016.
- (21) Akhavan, J. *The Chemistry of Explosives 4E*; Royal Society of Chemistry, 2022.
- (22) Balachandar, K. G.; Thangamani, A. Design of new energetic materials based on derivatives of 1, 3, 5-trinitrobenzenes: A theoretical and computational prediction of detonation properties, blast impulse and combustion parameters. *Heliyon* **2020**, *6* (1), e03163.
- (23) Kang, P.; Liu, Z.; Abou-Rachid, H.; Guo, H. Machine-learning assisted screening of energetic materials. *J. Phys. Chem. A* **2020**, *124* (26), 5341–5351.
- (24) Sivapirakasam, S. P.; Kumar, N. V.; Jeyabalaganesh, G.; Nagarjuna, K. Simple model for predicting the detonation velocity of organic, inorganic, and mixed explosives. *Combustion, Explosion, and Shock Waves* **2021**, *57* (6), 726–735.
- (25) Politzer, P.; Murray, J. S. The role of product composition in determining detonation velocity and detonation pressure. *Central European Journal of Energetic Materials* **2014**, *11* (4), 459–474.
- (26) Mader, C. L. *Detonation Performance Calculations Using the Kistiakowsky-Wilson Equation of State (Vol. 2613)*; Los Alamos Scientific Laboratory of the University of California, 1961.
- (27) Kim, H. J.; Lee, B. H.; Cho, S. G.; Lee, S. K. Comparative analysis of detonation velocity in determining product composition for high energetic molecules using stoichiometric rules. *Analytical Science and Technology* **2017**, *30* (6), 405–410.
- (28) Muthurajan, H.; Sivabalan, R.; Talawar, M. B.; Asthana, S. N. Computer simulation for prediction of performance and thermodynamic parameters of high energy materials. *Journal of hazardous materials* **2004**, *112* (1–2), 17–33.
- (29) Shukla, M.; Boddu, V. M.; Steevens, J. A.; Damavarapu, R.; Leszczynski, J. *Energetic materials (Vol. 482)*; Springer International Publishing, 2017.
- (30) *Molecular Operating Environment (MOE), 2018.01*; Chemical Computing Group ULC: Montreal, QC, Canada, 2018.
- (31) Berthold, M. R.; Cebren, N.; Dill, F.; Gabriel, T. R.; Kotter, T.; Meinel, T.; Ohl, P.; Thiel, K.; Wiswedel, B. KNIME-the Konstanz information miner: version 2.0 and beyond. *AcM SIGKDD explorations Newsletter* **2009**, *11* (1), 26–31.
- (32) Rayan, A.; Falah, M.; Raiyn, J.; Da'adoosh, B.; Kadan, S.; Zaid, H.; Goldblum, A. Indexing molecules for their hERG liability. *Eur. J. Med. Chem.* **2013**, *65*, 304–314.
- (33) El-Atawneh, S.; Goldblum, A. Iterative stochastic elimination for discovering hits and leads. *Chimica Oggi-Chemistry Today* **2017**, *35* (5), 41–46.

(34) Smith, M. E.; Wall, C.; Fitzgerald, M. Characterisation of the major synthetic products of the reactions between butanone and hydrogen peroxide. *Propellants, Explosives, Pyrotechnics* **2012**, *37* (3), 282–287.

(35) Gu, W.; Jiang, J. J.; Jiang, J. C.; Bin, L. *Thermal Instability and Kinetics Analysis on Triacetone Triperoxide (TATP)*; IOP Conference Series: Earth and Environmental Science; IOP Publishing, 2018; Vol. 189, No. 3, p.032046.

(36) Keshavarz, M. H.; Seif, F. Improved approach to predict the power of energetic materials. *Propellants, Explosives, Pyrotechnics* **2013**, *38* (5), 709–714.

(37) *Explosives Database*. <http://expdb.chm.uri.edu>.

(38) AIST. <https://www.aist.go.jp/>.

(39) Nazari, B.; Keshavarz, M. H.; Hamadani, M.; Mosavi, S.; Ghaedsharafi, A. R.; Pouretdal, H. R. Reliable prediction of the condensed (solid or liquid) phase enthalpy of formation of organic energetic materials at 298 K through their molecular structures. *Fluid Phase Equilib.* **2016**, *408*, 248–258.

(40) Willighagen, E. L.; Mayfield, J. W.; Alvarsson, J.; Berg, A.; Carlsson, L.; Jeliaskova, N.; Kuhn, S.; Pluskal, T.; Rojas-Cherto, M.; Spjuth, O.; et al. The Chemistry Development Kit (CDK) v2.0: atom typing, depiction, molecular formulas, and substructure searching. *Journal of cheminformatics* **2017**, *9*, 33.

(41) Shivanyuk, A. N.; Ryabukhin, S. V.; Tolmachev, A.; Bogolyubsky, A. V.; Mykytenko, D. M.; Chupryna, A. A.; Kostyuk, A. N. Enamine real database: Making chemical diversity real. *Chemistry today* **2007**, *25* (6), 58–59.